


Emergent antiferromagnetic transition in hyperkagome manganese $\text{Zn}_2\text{Mn}_3\text{O}_8$ Suguru Kitani^{1,*}, Takeshi Yajima,² and Hitoshi Kawaji¹¹Materials and Structures Laboratory, Tokyo Institute of Technology, 4259 Nagatsuta-cho, Midori-ku, Yokohama 226-8503, Japan²Institute for Solid State Physics, University of Tokyo, Kashiwa, Chiba, 277-8581, Japan (Received 26 February 2021; revised 15 April 2021; accepted 13 September 2021; published 27 September 2021)

We have successfully synthesized a hyperkagome antiferromagnet $\text{Zn}_2\text{Mn}_3\text{O}_8$ by a topochemical method, where Mn^{4+} ions with $S = 3/2$ spins form a three-dimensional (3D) corner-sharing triangle network. Magnetic susceptibility and heat capacity measurements revealed an antiferromagnetic transition at $T_N = 5.8$ K. Although no evidence was found for any structural distortion accompanying the transition, the low-temperature magnetic heat capacity showed a nearly T^2 dependence, suggesting the realization of a 2D magnonlike excitation in the 3D hyperkagome lattice.

DOI: [10.1103/PhysRevMaterials.5.094411](https://doi.org/10.1103/PhysRevMaterials.5.094411)

I. INTRODUCTION

Geometrically frustrated magnets have been intensively studied for decades because of the presence of various types of novel physical properties [1,2]. Spin frustration arising from strong competition between magnetic exchange interactions results in a macroscopically degenerated ground state, which may result in a spin-liquid state down to the lowest temperature [3]. Conversely, a weak perturbation in a real system often eliminates macroscopic degeneracy and releases frustration, leading to an exotic ground state. The platform for geometrical frustration is mostly based on triangle-based structures, such as triangular, kagome, and pyrochlore lattices. Among these lattices, the kagome lattice forming a corner-sharing triangular network has attracted much attention because of its high potential for hosting a spin liquid state, and extensive attention has been given to three Cu^{2+} minerals, i.e., herbertsmithite $\text{ZnCu}_3(\text{OH})_6\text{Cl}_2$ [4], volborthite $\text{Cu}_3\text{V}_2\text{O}_7(\text{OH})_2 \cdot 2\text{H}_2\text{O}$ [5], and vesignieite $\text{BaCu}_3\text{V}_2\text{O}_8(\text{OH})_2$ [6].

A three-dimensional (3D) analog of the kagome antiferromagnet, referred to as a hyperkagome antiferromagnet, is also a fascinating system. Sodium iridate $\text{Na}_4\text{Ir}_3\text{O}_8$ is a monumental compound of the hyperkagome antiferromagnet with spin $1/2$. $\text{Na}_4\text{Ir}_3\text{O}_8$ shows no clear evidence of macroscopic ordering down to at least 2 K [7], suggesting a quantum liquid ground state. However, muon spin rotation [8] and NMR experiments [9] for $\text{Na}_4\text{Ir}_3\text{O}_8$ have pointed out spin freezing at low temperatures, which may result from a local disorder associated with the partial occupancy of Na atoms [9]. Recently, the successful bulk single-crystal growth of $\text{Na}_4\text{Ir}_3\text{O}_8$ was reported [10], and further progress is expected in understanding its magnetic ground state. After discovering this material, numerous theoretical studies on the hyperkagome antiferromagnet have been reported, and they propose not only a spin liquid, but also an exotic ordered state as the ground state. The classical model suggests the emergence of

a nematic order [11]. In the semiclassical limit, a coplanar magnetically ordered ground state is predicted [12].

Other representative systems in the family of hyperkagome antiferromagnets are $\text{Gd}_3\text{Ga}_5\text{O}_{12}$ and $\text{PbCuTe}_2\text{O}_6$. Gadolinium garnet, $\text{Gd}_3\text{Ga}_5\text{O}_{12}$, is known as a system with two interpenetrating hyperkagome lattices of Gd^{3+} ($S = 7/2$). This compound shows no long-range order down to the lowest temperatures despite a Curie-Weiss temperature of -2.3 K [13,14], and a spin liquid ground state was confirmed by neutron scattering experiments [15]. The low-temperature phase of $\text{Gd}_3\text{Ga}_5\text{O}_{12}$ is of interest because of the cooperative magnetic multipolar degrees of freedom underlying the spin correlations [16] and a rich magnetic phase diagram [17]. $\text{PbCuTe}_2\text{O}_6$ realizes a hyperkagome magnetic lattice through the dominant second nearest-neighbor interaction between Cu^{2+} ions ($S = 1/2$) [18]. Magnetic susceptibility shows no sign of long-range order down to the lowest temperatures despite a Curie-Weiss temperature of -22 K. NMR and muon spin relaxation did not find any evidence of magnetic ordering down to 0.02 K, but a pronounced slowing down of the spin dynamics was observed below 1 K [19]. A recent single-crystal study revealed ferroelectric ordering at 1 K, accompanied by a lattice distortion, which could be the key to clarifying the quantum critical behavior in $\text{PbCuTe}_2\text{O}_6$ [20].

In this paper, we present the magnetic and thermal properties of an $S = 3/2$ hyperkagome antiferromagnet $\text{Zn}_2\text{Mn}_3\text{O}_8$. This compound can be prepared from the cubic spinel polymorph of $\text{Li}_2\text{ZnMn}_3\text{O}_8$ using a cation-exchange method [21]. Figure 1(a) shows the crystal structure of $\text{Li}_2\text{ZnMn}_3\text{O}_8$, and Fig. 1(c) shows the Mn and Li ions at the octahedral site, forming an ordered network of corner-shared tetrahedra. Three Mn and one Li ions occupy each tetrahedron, and the Mn ions form a corner-sharing triangular network, called a hyperkagome lattice. $\text{Li}_2\text{ZnMn}_3\text{O}_8$, however, has a ferromagnetic interaction between Mn ions ($\Theta_W = 38.5$ K) and undergoes a ferromagnetic transition at 22 K [23]. The $\text{Li}^+/\text{Zn}^{2+}$ cation-exchange reaction with $\text{Li}_2\text{ZnMn}_3\text{O}_8$ leads to the substitution of Li ions at the tetrahedral A site by Zn ions and the replacement of Li ions at the octahedral B site by vacancies,

*Corresponding author: kitani.s.aa@m.titech.ac.jp

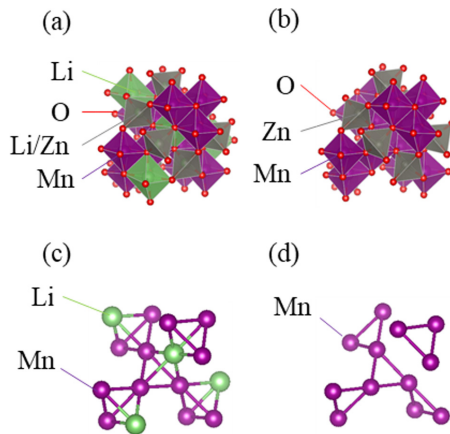


FIG. 1. Crystal structure of (a) $\text{Li}_2\text{ZnMn}_3\text{O}_8$ and (b) $\text{Zn}_2\text{Mn}_3\text{O}_8$ with the space group $P4_332$, illustrated by VESTA [22]. Purple and green octahedra represent MnO_6 and LiO_6 , and gray tetrahedra represent $(\text{Li}/\text{Zn})\text{O}_4$ or ZnO_4 . Network of ions in octahedral sites in (c) $\text{Li}_2\text{ZnMn}_3\text{O}_8$ and (d) $\text{Zn}_2\text{Mn}_3\text{O}_8$. From $\text{Li}_2\text{ZnMn}_3\text{O}_8$ to $\text{Zn}_2\text{Mn}_3\text{O}_8$, Li ions at the octahedral sites are replaced by vacancies, and the tetrahedral sites are occupied only by Zn ions. Accordingly, a corner-sharing *tetrahedral* network of Li and Mn ions in $\text{Li}_2\text{ZnMn}_3\text{O}_8$ changes to a corner-sharing *triangular* network, that is, a hyperkagome lattice in $\text{Zn}_2\text{Mn}_3\text{O}_8$.

as shown in Fig. 1(b). Magnetic Mn^{4+} ($t_{2g}^3 e_g^0$) ions maintain a triangular network through a cation-exchange reaction. To date, neither structural refinements nor physical property measurements have been performed for $\text{Zn}_2\text{Mn}_3\text{O}_8$. Our magnetic susceptibility measurements confirm that the exchange interaction is altered from ferromagnetic in $\text{Li}_2\text{ZnMn}_3\text{O}_8$ to antiferromagnetic in $\text{Zn}_2\text{Mn}_3\text{O}_8$, indicating the occurrence of geometrical frustration. Furthermore, magnetic susceptibility and heat capacity measurements reveal the antiferromagnetic transition at 5.8 K. As described above, although there are several hyperkagome antiferromagnets, none of the compounds showed any magnetic order. The first observation of the antiferromagnetic transition in hyperkagome antiferromagnets will lead to further developments in the study of hyperkagome antiferromagnets.

II. EXPERIMENTAL METHOD

Polycrystalline samples of $\text{Zn}_2\text{Mn}_3\text{O}_8$ were prepared by the cation-exchange reaction of $\text{Li}_2\text{ZnMn}_3\text{O}_8$ with $\text{ZnSO}_4 \cdot 7\text{H}_2\text{O}$. A powder precursor $\text{Li}_2\text{ZnMn}_3\text{O}_8$ with space group $P4_332$ was obtained by a conventional solid-state reaction [24,25]. For the cation-exchange reaction, a 1:15 molar ratio of $\text{Li}_2\text{ZnMn}_3\text{O}_8$ and $\text{ZnSO}_4 \cdot 7\text{H}_2\text{O}$ with a total mass of ~ 1 g was ground together and placed in an alumina crucible, followed by further stirring with added water. The crucible was heated in air around 100°C to evaporate the water and then at 230°C for 5 days. After this reaction, the product Li_2SO_4 and remnant ZnSO_4 were removed from the samples by washing with distilled water. The products were filtered and dried in air at 85°C . The procedure was repeated four times to complete the cation-exchange reaction. Successful cation-exchange without structural deformation was confirmed by powder x-ray diffraction (XRD). A Rietveld

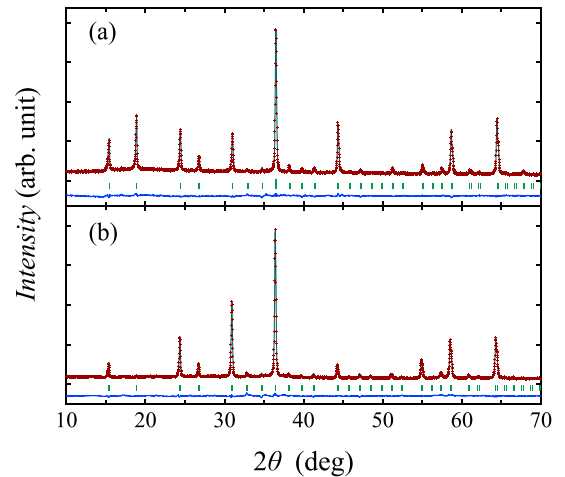


FIG. 2. Powder x-ray diffraction pattern of (a) $\text{Li}_2\text{ZnMn}_3\text{O}_8$ and (b) $\text{Zn}_2\text{Mn}_3\text{O}_8$ at room temperature. Red dots are experimental data, and green vertical bars indicate the positions of Bragg reflections. The green line on the data shows a calculated pattern with the space group $P4_332$, and the bottom blue line shows the difference between the experimental and calculated intensities.

analysis of the structural refinement was carried out using the Rietan-FP program [26]. Powder XRD experiments were also performed at low temperatures using a SmartLab (Rigaku). The incident x-ray beam was monochromated by a Johansson-type monochromator with a Ge(111) crystal to select only $\text{Cu-K}\alpha 1$ radiation. The heat capacity and magnetic properties were measured by the relaxation technique using a Quantum Design physical property measurement system (PPMS) and magnetic property measurement system (MPMS), respectively.

III. RESULTS AND DISCUSSION

The XRD patterns of polycrystalline $\text{Li}_2\text{ZnMn}_3\text{O}_8$ and $\text{Zn}_2\text{Mn}_3\text{O}_8$ samples at room temperature are shown in Fig. 2. The progress of the cation-exchange reaction is primarily characterized by strong suppression of the (111) peak near 20° , compared with the XRD pattern of $\text{Li}_2\text{ZnMn}_3\text{O}_8$. The structure was refined with the assumption that Li ions are equally distributed at the *A* and *B* sites, the number of Li ions is changed to maintain the total charge neutrality, and the isotropic thermal parameters of Li and O ions are unchanged from $\text{Li}_2\text{ZnMn}_3\text{O}_8$ [27]. Details of the refinement are given in Table I, and the obtained structure is presented in Fig. 1. The cation-exchange reaction extracted nearly all Li ions, which was also confirmed by ^6Li MAS NMR experiments. However, as described later, magnetic susceptibility measurements detected a small remnant of the precursor $\text{Li}_2\text{ZnMn}_3\text{O}_8$, which corresponded to the 0.7(1)% Li remaining in $\text{Zn}_2\text{Mn}_3\text{O}_8$. Note that the Rietveld refinement parameters were not improved by the assumptions of the random occupancy of the tetrahedral *A* and octahedral *B* sites by Zn ions and the displacement of Mn ions to the octahedral *B* site formerly occupied by Li ions.

Figure 3(a) shows the temperature dependence of the magnetic susceptibility χ below 100 K under various magnetic fields, where all curves showed a decrease below 5.8 K. The

TABLE I. Crystallographic parameters for $\text{Li}_2\text{ZnMn}_3\text{O}_8$ and $\text{Zn}_2\text{Mn}_3\text{O}_8$, obtained by Rietveld refinement against powder x-ray diffraction data for 10–140° collected at room temperature. During the refinement of $\text{Zn}_2\text{Mn}_3\text{O}_8$, the occupancies g of Zn, Li(1), and Li(2) were assumed such that Li ions are equally distributed at both sites and the number of Li ions is changed to keep the total charge neutral. Nevertheless, because the refined $g(\text{Zn})$ was 1.002(3), which agrees with 1 within the standard deviation, $g(\text{Zn})$ was fixed to 1 in the final refinement stage; hence Li(1) and Li(2) are not listed for $\text{Zn}_2\text{Mn}_3\text{O}_8$ in Table I.

| Atom | Site | x | y | z | g | $U_{\text{iso}} (\text{Å}^2)$ |
|---|------|------------|-----------|--------------|-----|-------------------------------|
| $\text{Li}_2\text{ZnMn}_3\text{O}_8$, $a = 8.185(1) \text{ Å}$, $R_{\text{wp}} = 1.67\%$, $S = 1.32$ | | | | | | |
| Zn | 8c | 0.0043(2) | $= x$ | $= x$ | 0.5 | 0.0155(5) |
| Li(1) | 8c | $= x$ (Zn) | $= x$ | $= x$ | 0.5 | 0.008 ^a |
| Li(2) | 4a | 5/8 | 5/8 | 5/8 | 1 | 0.020 ^a |
| Mn | 12d | 1/8 | 0.3757(2) | $= -y + 1/4$ | 1 | 0.0091(4) |
| O(1) | 8c | 0.3794(7) | $= x$ | $= x$ | 1 | 0.002(1) |
| O(2) | 24e | 0.1305(3) | 0.1544(7) | 0.8567(4) | 1 | 0.010(1) |
| $\text{Zn}_2\text{Mn}_3\text{O}_8$, $a = 8.203(1) \text{ Å}$, $R_{\text{wp}} = 1.95\%$, $S = 1.35$ | | | | | | |
| Zn | 8c | 0.0064(1) | $= x$ | $= x$ | 1 | 0.0054(4) |
| Mn | 12d | 1/8 | 0.3715(2) | $= -y + 1/4$ | 1 | 0.0025(4) |
| O(1) | 8c | 0.3891(1) | $= x$ | $= x$ | 1 | 0.008(2) |
| O(2) | 24e | 0.1252(4) | 0.1569(5) | 0.8652(5) | 1 | 0.014(2) |

^a U_{iso} of Li(1) and Li(2) was fixed to the value obtained by the neutron powder diffraction study [27].

inverse of χ , shown in Fig. 3(b), exhibited a linear temperature dependence above 100 K, following the Curie-Weiss law $\chi = C/(T - \Theta_{\text{W}})$, where C and Θ_{W} are the Curie constant and Weiss temperature, respectively. A Curie-Weiss fit to the $\chi(T)$ between 150 and 300 K leads to $C = 0.17 \text{ emu K g}^{-1}$ and $\Theta_{\text{W}} = -54 \text{ K}$, which gives a frustration index $f = |\Theta_{\text{W}}|/T_{\text{N}} \sim 9.3$. The value of C corresponds to the effective moments of $p_{\text{eff}} = 3.94 \mu_{\text{B}}/\text{Mn}^{4+}$, which is in good agree-

ment with the spin-only value for $S = 3/2$ of $p = 3.87 \mu_{\text{B}}$. The χ at 0.01 T showed a large hysteresis between field-cooling (FC) and zero-field-cooling (ZFC) procedures below 70 K and an appreciable rise at approximately 20 K, although these behaviors vanished with increasing applied magnetic field. This indicates that magnetic fields suppressed the ferromagnetic component induced by the residual $\text{Li}_2\text{ZnMn}_3\text{O}_8$ having a ferromagnetic transition near the same temperature [28]. The effect of the residual was also observed in the M - H curve at $T = 4.2 \text{ K}$ in Fig. 3(c) as a tiny kink near zero magnetic field. Above 1 T, the ferromagnetic component becomes saturated, and M exhibits a linear dependence on the magnetic field, suggesting that the antiferromagnetic phase is stable at least up to 5 T.

The negative value of Θ_{W} indicates that the dominant magnetic interaction is antiferromagnetic, thus the magnetic transition at 5.8 K is the antiferromagnetic transition. Based on the molecular field approximation with the nearest-neighbor interaction, the exchange constant $J = -3k_{\text{B}}\Theta_{\text{W}}/zS(S+1)$ is related to $|\Theta_{\text{W}}|$, where z is the number of nearest-neighbor atoms. According to this equation, the experimental value $\Theta_{\text{W}} = -54 \text{ K}$ for $\text{Zn}_2\text{Mn}_3\text{O}_8$ with $z = 4$ leads to $J/k_{\text{B}} = 10.8 \text{ K}$. The reason why the ferromagnetic interaction in $\text{Li}_2\text{ZnMn}_3\text{O}_8$ turns to be antiferromagnetic in $\text{Zn}_2\text{Mn}_3\text{O}_8$ is not clear so far. The magnetic properties of these materials result essentially from (1) the direct exchange interaction between the Mn^{4+} - Mn^{4+} ions and thus is related to their bond distance, and (2) the 90° superexchange interaction of Mn^{4+} - O^{2-} - Mn^{4+} , which is related to their bond angle [29,30]. The cation exchange expands the Mn-Mn distance from 2.89 Å in $\text{Li}_2\text{ZnMn}_3\text{O}_8$ to 2.92 Å in $\text{Zn}_2\text{Mn}_3\text{O}_8$. This expansion weakens the antiferromagnetic interaction because the direct overlap of d orbitals becomes small. The Mn-O-Mn angles are 92.1° and 100.7° in $\text{Li}_2\text{ZnMn}_3\text{O}_8$ and 90.2° and 101.9° in $\text{Zn}_2\text{Mn}_3\text{O}_8$, suggesting that the magnitude of the 90° Mn-O-Mn ferromagnetic superexchange interaction is almost the same. Hence, the ferromagnetic interaction in $\text{Li}_2\text{ZnMn}_3\text{O}_8$ may result from a complex Mn-O-Li-O-Mn superexchange interaction through Li ions.

Figure 4(a) shows the magnetic heat capacity C_m of $\text{Zn}_2\text{Mn}_3\text{O}_8$, which was obtained by subtracting the lattice heat capacity estimated from the nonmagnetic isostructural $\text{Zn}_2\text{Ge}_3\text{O}_8$ [31]. The antiferromagnetic phase transition appears as a sharp peak at the T_{N} . This peak did not exhibit thermal hysteresis, suggesting a second-order nature. C_m persists to a considerably higher temperature than T_{N} , as frequently observed in geometrically frustrated magnets. The magnetic entropy S_m , shown in Fig. 4(b), was estimated by integrating $C_m T^{-1}$. A large entropy release above T_{N} is a characteristic behavior of a frustrated system. The S_m reaches $27.0 \text{ J mol}^{-1} \text{ K}^{-1}$ at 100 K, corresponding to approximately 80% of the theoretical transition entropy for the $S = 3/2$ magnet, $S = 3R \ln 4 = 34.6 \text{ J mol}^{-1} \text{ K}^{-1}$. The lack of entropy is often caused by baseline estimates. However, as discussed below, $\text{Zn}_2\text{Mn}_3\text{O}_8$ does not have a strong spin-lattice coupling, so the lattice vibrations of $\text{Zn}_2\text{Mn}_3\text{O}_8$ and $\text{Zn}_2\text{Ge}_3\text{O}_8$ would not be significantly different. We also attempted to estimate the lattice heat capacity by fitting to the C_p in the high-temperature region with a combined Einstein-Debye model, although the obtained S_m was almost the same. Thus, the

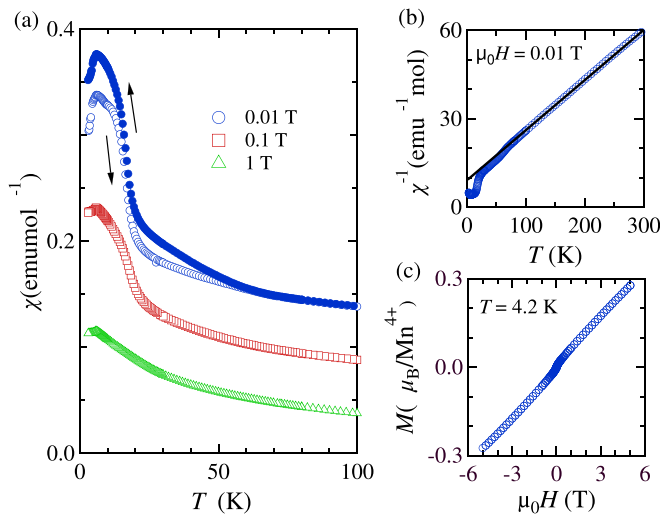


FIG. 3. (a) Temperature dependence of the magnetic susceptibility χ under fields of 0.01, 0.1, and 1 T. The χ curves measured at 0.01 and 0.1 T are shifted for clarity. (b) Temperature dependence of the inverse magnetic susceptibility χ^{-1} under 0.01 T, where the solid line indicates a Curie-Weiss fit. (c) Magnetization vs applied magnetic field for $\text{Zn}_2\text{Mn}_3\text{O}_8$ measured at 4.2 K.

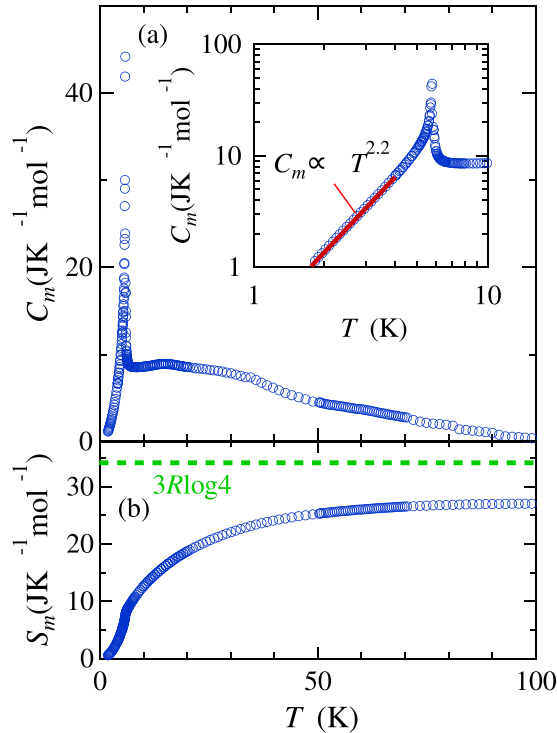


FIG. 4. (a) Magnetic heat capacity C_m of $\text{Zn}_2\text{Mn}_3\text{O}_8$, estimated by subtracting the lattice heat capacity calculated by scaling C_p of $\text{Zn}_2\text{Ge}_3\text{O}_8$ from the C_p . The inset displays the power-law behavior of C_m . (b) Magnetic entropy of $\text{Zn}_2\text{Mn}_3\text{O}_8$. The horizontal broken line corresponds to $S_m = 3R\ln 4$, which is expected for a fully ordered $S = 3/2$ system.

baseline is unlikely to be a problem, and $\text{Zn}_2\text{Mn}_3\text{O}_8$ would have a disorder or degeneracy in the ground state.

To consider the observed antiferromagnetic transition, we will explore the geometrically frustrated spinel system CdCr_2O_4 , forming a corner-sharing tetrahedral network, called the pyrochlore lattice, of Cr^{3+} ions. The hyperkagome lattice can be viewed as an ordered structure of the pyrochlore lattice with a ratio of 1:3, hence the chemical formula of $\text{Zn}_2\text{Mn}_3\text{O}_8$ is rewritten as $\text{Zn}(\square_{0.5}\text{Mn}_{1.5})_2\text{O}_4$, where \square denotes the vacancy. In addition to the structural analogy, both magnetic Cr^{3+} and Mn^{4+} ions have the same electronic state of half-filled t_{2g} and empty e_g orbitals ($t_{2g}^3 e_g^0$), being $S = 3/2$ with no orbital degrees of freedom, and the antiferromagnetic transition temperature $T_N = 7.8$ K and the exchange constant $J/k_B \sim 11.7$ K of CdCr_2O_4 [32] are also similar to those of $\text{Zn}_2\text{Mn}_3\text{O}_8$ ($T_N = 5.8$ K, $J/k_B = 10.8$ K). In the case of CdCr_2O_4 , the lattice plays an important role in relieving the geometrical frustration because of the lack of orbital degrees of freedom, resulting in lattice distortion at the antiferromagnetic transition [33]. Thus, we suspected lattice distortion at the T_N of $\text{Zn}_2\text{Mn}_3\text{O}_8$ and carried out low-temperature x-ray diffraction measurements. However, the XRD patterns below T_N were almost the same as those in Fig. 2(b). The XRD patterns at the high-angle side showed no peak splitting and no change in the FWHM above and below T_N , as shown in Fig. 5, which provides strong evidence for the lack of any structural distortion. This result suggests that the ground state

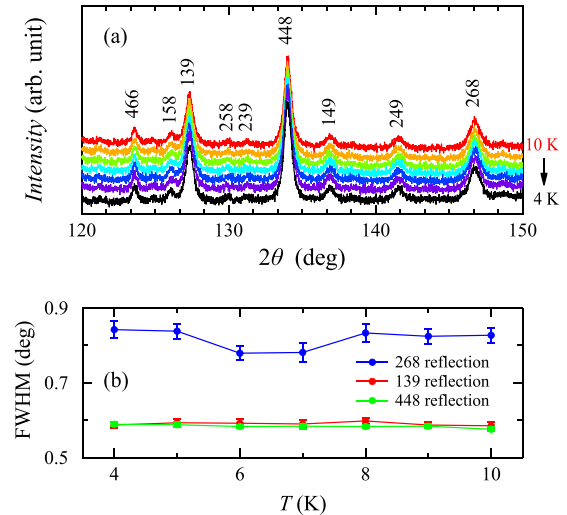


FIG. 5. (a) Temperature evolution of the low-temperature powder x-ray diffraction pattern at the high angle side, ranging from 10 to 4 K in 1-K increments. (b) Temperature dependences of full width at half maximum (FWHM) for selected diffraction peaks.

is a unique magnetic structure arising from the hyperkagome lattice.

Various theoretical studies on hyperkagome antiferromagnets have been performed to find a possible quantum spin liquid state in $\text{Na}_4\text{Ir}_3\text{O}_8$ [11,12,34–49]. Among them, the following three classical Heisenberg models are possible for $\text{Zn}_2\text{Mn}_3\text{O}_8$, because $\text{Zn}_2\text{Mn}_3\text{O}_8$ has a less quantum nature, no orbital degrees of freedom, and an apparent phase transition. The first model investigates the classical Heisenberg model with only the nearest-neighbor interaction [11], suggesting a nematic transition at $T \sim J/1000$, where J is the nearest-neighbor interaction. Then, the nematic transition temperature $J/1000$ in $\text{Zn}_2\text{Mn}_3\text{O}_8$ is ~ 0.01 K, which is not compatible with observation, hence this scenario can be excluded. The second includes the next nearest-neighbor interaction J_2 , i.e., the J_1 - J_2 model [39]. Considering that the precursor of $\text{Zn}_2\text{Mn}_3\text{O}_8$ was ferromagnetic $\text{Li}_2\text{ZnMn}_3\text{O}_8$, J_2 might be ferromagnetic because of the 90° Mn-O-Mn exchange. Thus, $\text{Zn}_2\text{Mn}_3\text{O}_8$ has $J_1 < 0$ and $J_2 > 0$, which results in a coplanar 120° order. The last model introduces the effects of anisotropic interactions [40]. Although anisotropic interactions result from spin-orbital interactions, such as Hund's coupling and spin-orbit coupling, there is a system with no orbital degrees of freedom where the chiral nature of the lattice generates relativistic spin-orbit coupling, resulting in the Dzyaloshinskii-Moriya interaction [50]. This kind of interaction might also occur in $\text{Zn}_2\text{Mn}_3\text{O}_8$ because the inversion symmetry of its lattice is broken. In such a case, the theoretical model predicts the doubly degenerate windmill states, forming a 120° structure. Nevertheless, further studies are needed to reveal the type of magnetic structure that has been established.

Finally, the temperature dependence of the low-temperature heat capacity is presented in the inset of Fig. 4(a). The C_m of $\text{Zn}_2\text{Mn}_3\text{O}_8$ varied as $T^{2.2}$ below 4 K, which is considerably smaller than the cubic dependence

seen in the normal 3D antiferromagnet, rather close to the square dependence seen in the 2D antiferromagnet. Nevertheless, the 3D hyperkagome structure in $\text{Zn}_2\text{Mn}_3\text{O}_8$ was maintained in the antiferromagnetic phase, as observed in the low-temperature XRD patterns (Fig. 5). Thus, this behavior implies the presence of a 2D magnonlike dispersion in the 3D hyperkagome antiferromagnet $\text{Zn}_2\text{Mn}_3\text{O}_8$. Intriguingly, nearly T^2 dependence in the low-temperature C_m can also be seen in the $S = 1/2$ hyperkagome antiferromagnet $\text{Na}_4\text{Ir}_3\text{O}_8$ [7]. A theoretical study was proposed for $\text{Na}_4\text{Ir}_3\text{O}_8$ where the instability of the spinon Fermi surface in a spin liquid state induces the T^2 dependence [12], although a recent NMR study showed that the ground state of $\text{Na}_4\text{Ir}_3\text{O}_8$ is no longer a spin liquid, but a spin-freezing state [9]. This scenario cannot be applied to $\text{Zn}_2\text{Mn}_3\text{O}_8$ in an antiferromagnetically ordered state. The reason why a 2D magnonlike dispersion appears in the 3D lattice is a fascinating subject for future studies, and examining the relevance of $\text{Zn}_2\text{Mn}_3\text{O}_8$ and $\text{Na}_4\text{Ir}_3\text{O}_8$ will provide further understanding of magnetism in the hyperkagome lattice.

IV. SUMMARY

In summary, we have investigated a hyperkagome antiferromagnet $\text{Zn}_2\text{Mn}_3\text{O}_8$ with the $S = 3/2$ using heat capacity and magnetic susceptibility measurements. $\text{Zn}_2\text{Mn}_3\text{O}_8$ exhibits an antiferromagnetic transition at $T_N = 5.8$ K, although other hyperkagome antiferromagnets do not show an apparent phase transition. Interestingly, the low-temperature heat capacity showed the temperature dependence expected for a 2D antiferromagnet, even though there was no structural phase transition. These results suggest that the magnon excitation of the antiferromagnetic phase in $\text{Zn}_2\text{Mn}_3\text{O}_8$ is significantly different from that of other 3D frustrated magnets, and $\text{Zn}_2\text{Mn}_3\text{O}_8$ is a model compound for studying antiferromagnetic ordering in the hyperkagome lattice.

ACKNOWLEDGMENT

This work was supported by JSPS KAKENHI Grant No. JP20K15019.

-
- [1] A. P. Ramirez, *Annu. Rev. Mater. Sci.* **24**, 453 (1994).
 [2] O. A. Starykh, *Rep. Prog. Phys.* **78**, 052502 (2015).
 [3] L. Balents, *Nature (London)* **464**, 199 (2010).
 [4] M. P. Shores, E. A. Nytko, B. M. Bartlett, and D. G. Nocera, *J. Am. Chem. Soc.* **127**, 13462 (2005).
 [5] Z. Hiroi, M. Hanawa, N. Kobayashi, M. Nohara, H. Takagi, Y. Kato, and M. Takigawa, *J. Phys. Soc. Jpn.* **70**, 3377 (2001).
 [6] Y. Okamoto, H. Yoshida, and Z. Hiroi, *J. Phys. Soc. Jpn.* **78**, 033701 (2009).
 [7] Y. Okamoto, M. Nohara, H. Aruga-Katori, and H. Takagi, *Phys. Rev. Lett.* **99**, 137207 (2007).
 [8] R. Dally, T. Hogan, A. Amato, H. Luetkens, C. Baines, J. Rodriguez-Rivera, M. J. Graf, and S. D. Wilson, *Phys. Rev. Lett.* **113**, 247601 (2014).
 [9] A. C. Shockley, F. Bert, J. C. Orain, Y. Okamoto, and P. Mendels, *Phys. Rev. Lett.* **115**, 047201 (2015).
 [10] H. Zheng, J. Zhang, C. C. Stoumpos, Y. Ren, Y. Chen, R. Dally, S. D. Wilson, Z. Islam, and J. F. Mitchell, *Phys. Rev. Materials* **2**, 043403 (2018).
 [11] J. M. Hopkinson, S. V. Isakov, H. Y. Kee, and Y. B. Kim, *Phys. Rev. Lett.* **99**, 037201 (2007).
 [12] M. J. Lawler, A. Paramakanti, Y. B. Kim, and L. Balents, *Phys. Rev. Lett.* **101**, 197202 (2008).
 [13] S. Hov, H. Bratsberg, and A. T. Skjeltorp, *J. Magn. Magn. Mater.* **15–18**, 455 (1980).
 [14] A. P. Ramirez and R. N. Kleiman, *J. Appl. Phys.* **69**, 5252 (1991).
 [15] O. A. Petrenko, C. Ritter, M. Yethiraj, and D. McK. Paul, *Phys. Rev. Lett.* **80**, 4570 (1998).
 [16] J. A. M. Paddison, H. Jacobsen, O. A. Petrenko, M. Teresa Fernández-Díaz, P. P. Deen, and A. L. Goodwin, *Science* **350**, 179 (2015).
 [17] A. Rousseau, J. M. Parent, and J. A. Quilliam, *Phys. Rev. B* **96**, 060411(R) (2017).
 [18] B. Koteswararao, R. Kumar, P. Khuntia, S. Bhowal, S. K. Panda, M. R. Rahman, A. V. Mahajan, I. Dasgupta, M. Baenitz, K. H. Kim, and F. C. Chou, *Phys. Rev. B* **90**, 035141 (2014).
 [19] P. Khuntia, F. Bert, P. Mendels, B. Koteswararao, A. V. Mahajan, M. Baenitz, F. C. Chou, C. Baines, A. Amato, and Y. Furukawa, *Phys. Rev. Lett.* **116**, 107203 (2016).
 [20] C. Thurn, P. Eibisch, A. Ata, U. Tutsch, Y. Saito, S. Hartmann, J. Zimmermann, A. R. N. Hanna, A. T. M. N. Islam, S. Chillal, B. Lake, B. Wolf, and M. Lang, *arXiv:2103.17175*.
 [21] J. C. Joubert and A. Durif, *Bull. Soc. Fr. Miner. Cristal.* **90**, 598 (1967).
 [22] K. Momma and F. Izumi, *J. Appl. Crystallogr.* **44**, 1272 (2011).
 [23] R. Plumier and M. Sougi, *J. Appl. Phys.* **67**, 4787 (1990).
 [24] G. J. Blasse, *J. Inorg. Nucl. Chem.* **26**, 1473 (1964).
 [25] J. C. Joubert and A. Durif, *Compt. Rend.* **258**, 4482 (1964).
 [26] F. Izumi and K. Momma, *Solid State Phenom.* **130**, 15 (2007).
 [27] Y. J. Lee, S.-H. Park, C. Eng, J. B. Parise, and C. P. Grey, *Chem. Mater.* **14**, 194 (2002).
 [28] G. Blasse, *J. Phys. Chem. Solids* **27**, 383 (1966).
 [29] J. Kanamori, *J. Phys. Chem. Solids* **10**, 87 (1959).
 [30] J. B. Goodenough, *Magnetism and the Chemical Bond* (Interscience, New York, 1963).
 [31] J. C. Joubert and A. Durif, *Bull. Soc. fr. Mineral. Cristallogr.* **87**, 517 (1964).
 [32] J. H. Chung, M. Matsuda, S. H. Lee, K. Kakurai, H. Ueda, T. J. Sato, H. Takagi, K. P. Hong, and S. Park, *Phys. Rev. Lett.* **95**, 247204 (2005).
 [33] M. T. Rovers, P. P. Kyriakou, H. A. Dabkowska, G. M. Luke, M. I. Larkin, and A. T. Savici, *Phys. Rev. B* **66**, 174434 (2002).
 [34] D. Podolsky and Y. B. Kim, *Phys. Rev. B* **83**, 054401 (2011).
 [35] G. Chen and Y. B. Kim, *Phys. Rev. B* **87**, 165120 (2013).
 [36] R. R. P. Singh and J. Oitmaa, *Phys. Rev. B* **85**, 104406 (2012).
 [37] I. Kimchi and A. Vishwanath, *Phys. Rev. B* **89**, 014414 (2014).
 [38] R. Shindou, *Phys. Rev. B* **93**, 094419 (2016).
 [39] F. L. Buessen and S. Trebst, *Phys. Rev. B* **94**, 235138 (2016).
 [40] T. Mizoguchi, K. Hwang, E. K.-H. Lee, and Y. B. Kim, *Phys. Rev. B* **94**, 064416 (2016).
 [41] B. Huang, Y. B. Kim, and Y. M. Lu, *Phys. Rev. B* **95**, 054404 (2017).

- [42] M. J. Lawler, H. Y. Kee, Y. B. Kim, and A. Vishwanath, *Phys. Rev. Lett.* **100**, 227201 (2008).
- [43] Y. Zhou, P. A. Lee, T. K. Ng, and F. C. Zhang, *Phys. Rev. Lett.* **101**, 197201 (2008).
- [44] G. Chen and L. Balents, *Phys. Rev. B* **78**, 094403 (2008).
- [45] D. Podolsky, A. Paramekanti, Y. B. Kim, and T. Senthil, *Phys. Rev. Lett.* **102**, 186401 (2009).
- [46] M. Udagawa and Y. Motome, *J. Phys. Conf. Ser.* **145**, 012013 (2009).
- [47] M. R. Norman and T. Micklitz, *Phys. Rev. B* **81**, 024428 (2010).
- [48] T. Micklitz and M. R. Norman, *Phys. Rev. B* **81**, 174417 (2010).
- [49] E. J. Bergholtz, A. M. Läuchli, and R. Moessner, *Phys. Rev. Lett.* **105**, 237202 (2010).
- [50] G. W. Chern, C. J. Fennie, and O. Tchernyshyov, *Phys. Rev. B* **74**, 060405(R) (2006).